Journal of Materials Chemistry A

COMMUNICATION

View Article Online
View Journal | View Issue

Cite this: J. Mater. Chem. A, 2015, 3, 1915

Received 18th November 2014
Accepted 22nd December 2014

DOI: 10.1039/c4ta06284a

www.rsc.org/MaterialsA

N-doped carbon-coated cobalt nanorod arrays supported on a titanium mesh as highly active electrocatalysts for the hydrogen evolution reaction†

Weijia Zhou,*[a] Yucheng Zhou,[a] Linjing Yang,[a] Jilin Huang,[a] Yunting Ke,[a] Kai Zhou,[a] Ligui Li[a] and Shaowei Chen*[ab]

N-doped carbon-coated cobalt nanorod arrays supported on a Ti mesh were prepared by a two-step procedure involving hydrothermal synthesis of Co_3O_4 nanorods followed by thermal reduction to metallic cobalt. The nanocomposites exhibited a remarkable catalytic activity that was comparable to that of leading commercial Pt/C catalysts.

Development of effective technologies for clean and sustainable hydrogen energy has attracted great attention recently, as hydrogen is hailed as a promising energy source to reduce our dependence on fossil fuels and benefit the environment by reducing the emissions of greenhouse and other toxic gases. To this end, an effective and promising approach is based on the electrolysis of water for hydrogen production.[1–3] In these studies, advanced catalysts for the electrochemical hydrogen evolution reaction (HER) are required to achieve high current density at low overpotentials.[4–6] Although platinum group metals are currently the electrocatalysts of choice that exhibit almost no overpotential,[7] the scarcity and high costs of platinum severely limit its widespread applications in the HER, and it has remained a great challenge to develop highly active HER catalysts based on abundant materials (such as carbon and transition metals) with a low overpotential.[8–13]

As acidic solutions are preferred for water electrolysis to produce hydrogen, HER catalysts need to be acid-stable. Molybdenum- and tungsten-based compounds are an exciting family of HER catalysts with a high performance, including MoS_2,[14–17] $MoSe_2$,[18] Mo_2C,[19] $NiMoN_x$,[20] MoP,[21] and WS_2,[22] which exhibit excellent activity and robust stability in acidic electrolytes. A remarkable HER activity has also been observed with other transition-metal compounds, such as $CoSe_2$,[23] CoS_2,[24] CoP,[25] NiP,[26] and CuP.[27] Of these, reports have been relatively scarce where transition metals of Co, Fe and Ni are actually used for the preparation of HER catalysts largely because of their chemical instability in acidic environments, although some progress has been made recently. For instance, Zou *et al.*[28] recently described the synthesis of cobalt-embedded nitrogen-rich carbon nanotubes (CNTs), which were found to exhibit apparent electrocatalytic activity for the HER in a wide range of pH, with a small onset potential of −50 mV and a low Tafel slope (69 mV dec^{-1}) in 0.5 M H_2SO_4. Successes like this highlight the possibility of using transition metals (*e.g.*, Co, Ni, *etc.*) as the active components for HER electrocatalysis in acidic electrolytes, which will significantly expand the "tool box" for the design and engineering of HER catalysts.[28–30]

Notably, to develop HER electrodes that are of high efficiency, low costs, and binder-free, active components are in general directly grown on current-collecting substrates instead of using Nafion or PTFE to immobilize catalysts on electrode surfaces. In recent years, a variety of self-supported 3D nanoarrays, such as 3D CoO@polypyrrole nanowire arrays,[31] Ni_3S_2 nanorods, FeP,[32] *etc.*, have been constructed on current collectors that exhibit vectorial electron-transport characteristics and high electrochemical surface areas.[33–35] For instance, Sun *et al.*[25] reported the topotactic fabrication of self-supported nanoporous cobalt phosphide nanowire arrays on carbon cloth (CoP/CC) *via* low-temperature phosphidation of the corresponding Co(OH)F/CC precursor. The obtained CoP/CC, as a robust integrated 3D hydrogen-evolving cathode, showed a low onset potential of −38 mV and a small Tafel slope of 51 mV dec^{-1}, and maintained its catalytic activity for at least 80 000 s in acidic media.

Herein, we describe the preparation of self-supported N-doped carbon-coated cobalt nanorod arrays supported on a Ti mesh (Co@NC/Ti), which exhibited a remarkable HER performance in acid solutions. Experimentally, Co_3O_4 nanorod arrays were first grown directly on a Ti mesh by a hydrothermal route and subsequently reduced to Co with a carbon overcoating layer

[a]New Energy Research Institute, School of Environment and Energy, South China University of Technology, Guangzhou Higher Education Mega Center, Guangzhou, Guangdong 510006, China. E-mail: eszhouwj@scut.edu.cn; shaowei@ucsc.edu

[b]Department of Chemistry and Biochemistry, University of California, 1156 High Street, Santa Cruz, California 95064, USA

† Electronic supplementary information (ESI) available: Experimental details, and additional data and discussion. See DOI: 10.1039/c4ta06284a

by thermal decomposition of dicyanodiamine. The Co@NC/Ti electrode exhibited apparent HER activity in 0.5 M H_2SO_4, with an onset overpotential of −56 mV, a Tafel slope of 78.2 mV dec^{-1}, and robust stability for 8 h of continuous operation. This was ascribed to the carbon shell that protected the cobalt nanorods from dissolution in highly acidic 0.5 M H_2SO_4 as well as to the catalytic contributions from surface carbons that were mediated by the entrapped Co nanoparticles as a result of interfacial charge transfer.

The synthesis process of Co@NC/Ti is depicted in Fig. 1 which entails the following major steps (details in the ESI†): (a) $Co(OH)_2$ nanowires were grown on the Ti mesh surface *via* a hydrothermal process; (b) calcination of the $Co(OH)_2$ nanowires at 450 °C in air led to the production of porous Co_3O_4 nanorods; (c) dicyanodiamine was adsorbed onto the surface of Co_3O_4 nanorods; and (d) Co_3O_4 nanorods were reduced to Co nanorods at 700 °C in an Ar atmosphere by carbon generated from thermal decomposition of dicyanodiamine; meanwhile, the graphitic carbon formed an overcoating layer on the Co surface.[28] Of note is that the carbon layer was self-doped with nitrogen that originated from dicyanodiamine.

Further structural characterization was carried out by TEM measurements. Fig. 2a and b show the top-view and side-view SEM micrographs of Co@NC nanorod arrays supported on a Ti mesh, respectively. It can be seen that the entire surface of the Ti mesh was covered uniformly by a densely packed Co@NC nanorod array. The size of the Co@NC nanorods was found to be about 300–400 nm in diameter, and 2 to 3 μm in length. In comparison, the Co_3O_4 nanorods before reduction were somewhat smaller with 50–150 nm in diameter (Fig. S1†), with the elemental composition confirmed by energy dispersive X-ray (EDX) analysis, as depicted in Fig. S2.† XRD measurements (Fig. 2c) show two major peaks at 44.35° and 51.64° (indicated by asterisks) that are characteristic of metallic Co (111) and (200) (JCPDS no. 15-0806), respectively. Additional diffraction peaks can be seen at 36.3°, 38.4°, 40.28°, 54.43°, 62.93°, 69.14° and 75.99° (marked by the number signs) that most likely originated from the Ti mesh substrate (JCPDS no. 44-1294). This is in marked contrast with the diffraction patterns of Co_3O_4/Ti (Fig. S1c†). Fig. 2d shows the TEM image of a single Co@NC nanorod, where one can see a core–shell structure with different contrasts. In fact, the high-resolution image in Fig. 2e clearly shows a three-layer structure in the Co@NC nanorod. First, the core part showed well-resolved lattice fringes with an interplanar distance of 0.20 nm that was consistent with the Co(111)

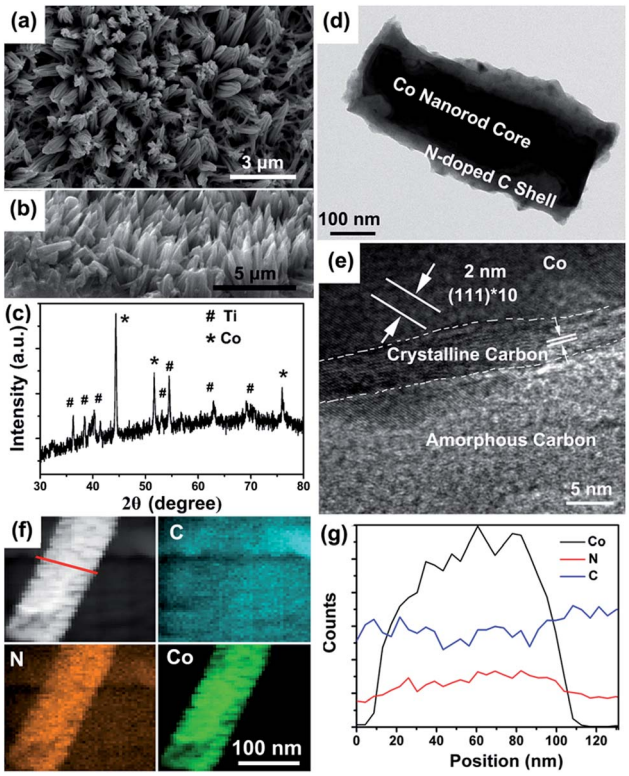

Fig. 2 (a) Top view and (b) side-view SEM images, (c) XRD patterns and (d and e) TEM images of Co@NC/Ti. (f) The corresponding EDX elemental mapping images of C, N and Co for Co@NC. (g) EDX line scan curves showing C, N, and Co element profiles across the Co@NC indicated by the red line in (f).

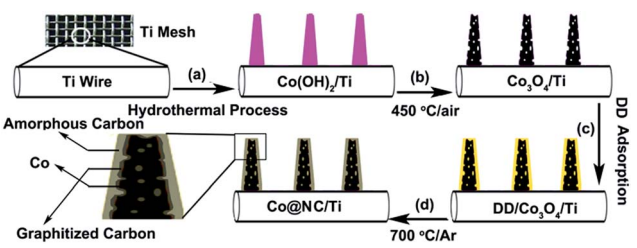

Fig. 1 Schematic of the synthesis of Co@NC/Ti. DD denotes dicyanodiamine.

planes. Second, on the immediate surface of the Co nanorod, a crystalline overcoating shell can be seen which exhibited an interplanar distance of 0.34 nm that was in good agreement with the (002) planes of graphitic carbon. Third, the outermost layer appeared to consist of amorphous carbon. This carbon layer most likely originated from the thermal decomposition of cyanamide and reduced Co_3O_4 to Co at elevated temperatures. Similar results have been reported previously in the synthesis of carbon nanotubes and graphene nanosheets.[28,36,37] In contrast, before calcination with dicyanodiamine, the Co_3O_4 nanorods showed only a crystalline phase with an interplanar distance of 0.24 nm, corresponding to the Co_3O_4 (311) crystalline planes (Fig. S3†). Furthermore, in panel (f), elemental mapping analysis of a single hybrid Co@NC nanorod showed that the elements C, N, and Co were distributed rather homogeneously throughout the entire nanorod. Nevertheless, line scans across the nanorods (indicated by the red line in Fig. 2f) signified the formation of a core–shell structure. From panel (g), one can see that the concentration of Co peaked at the center of the nanorod whereas those of C and N at the edges.

XPS measurements were then carried out to further evaluate the chemical compositions and valence states of the nanocomposites. Fig. 3a shows the survey spectrum of Co@NC/Ti, where the elements Ti, Co, C and N can be readily identified. Fig. 3b depicts the high-resolution scan of the Co2p electrons which exhibited a doublet at 795.1 eV and 780.2 eV.

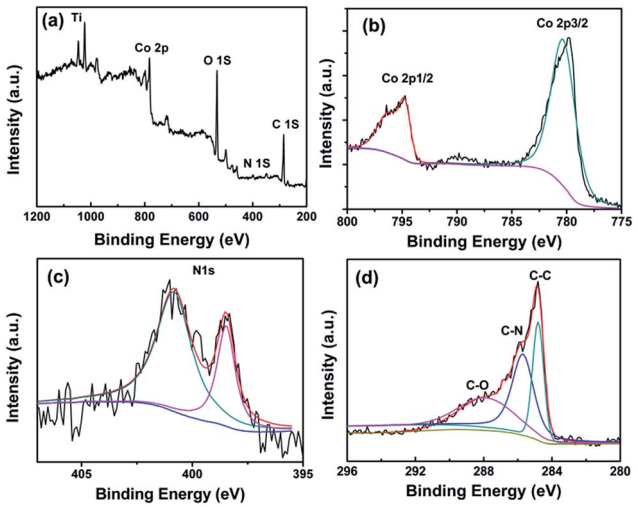

Fig. 3 (a) XPS survey spectra and high-resolution scans of (b) Co2p, (c) C1s and (d) N1s electrons of Co@NC/Ti.

Deconvolution of the high-resolution scan of the N1s electrons yielded two peaks at 398.4 and 401.2 eV (Fig. 3c) that are consistent with the pyridinic and pyrrolic nitrogen, respectively, indicating the successful incorporation of N into the graphitic matrix with a N-doping content of 3.36 at%.[38] In addition, the N doping was also observed in the survey spectra of the C element as shown in Fig. 3b, where the C–N characteristic peak can be identified at 286.1 eV.

The HER activity of the nanocomposites prepared above was then examined by electrochemical measurements in highly acidic media. Fig. 4a shows the polarization curve of Co@NC/Ti (at a loading of 11.2 mg cm^{-2}) in 0.5 M H_2SO_4 at a scan rate of 5 mV s^{-1}. A blank Ti mesh, Co_3O_4/Ti (at a loading of 8.7 mg cm^{-2}), Co/Ti (at a loading of 7.1 mg cm^{-2}) and 20 wt% Pt/C on a Ti mesh (at a loading of 11.2 mg cm^{-2}) were also examined for comparison. The blank Ti mesh and Co_3O_4/Ti mesh showed poor HER activity with almost no reduction current until the electrode potentials were more negative than −458 mV and −245 mV, respectively. Furthermore, for Co/Ti, that was prepared by H_2 reduction of Co_3O_4/Ti at 600 °C and hence without a carbon coating layer (Fig. S4†), the HER activity was also low with an onset potential of −253 mV. In sharp contrast, Co@NC/Ti was significantly more active for the HER with an onset potential of only −56 mV, which is close to that of commercial Pt/C (−12 mV). Increasingly negative potentials led to a rapid rise of the cathodic current. For instance, the current densities increased by 10 fold from 10 to 100 mA cm^{-2} when the Co@NC/Ti electrode potential swept cathodically by less than 80 mV from −106 mV to −184 mV. This indicates the significance of the carbon coating layer in the determination of the HER activity.

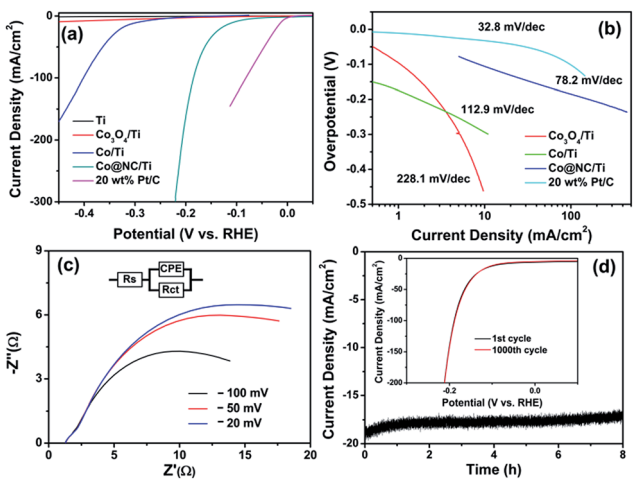

Fig. 4 (a) Polarization curves for the HER in 0.5 M H_2SO_4 at a Ti mesh, Co_3O_4/Ti, Co/Ti, Co@NC/Ti and 20 wt% Pt/C on a Ti mesh. Potential sweep rate 5 mV s^{-1}. (b) Corresponding Tafel plots (overpotential *versus* log current density) derived from (a). (c) Nyquist plots and the equivalent circuit of Co@NC/Ti at various HER overpotentials in 0.5 M H_2SO_4. (d) Current–time plots of the Co@NC/Ti electrode at an applied potential of −0.15 V (*vs.* RHE). The inset is the HER polarization curves for Co@NC/Ti before and after 1000 cycles in the stability test.

Furthermore, the linear portions of the polarization curves were fitted to the Tafel equation ($\eta = b \log j + a$, where j is the current density and b is the Tafel slope), yielding a Tafel slope of 78.2 mV dec^{-1} for Co@NC/Ti and 32.8 mV dec^{-1} for 20 wt% Pt/C (Fig. 4b), signifying that the HER proceeded by a Volmer–Heyrovsky mechanism on Co@NC/Ti.[17,39] Note that a much higher Tafel slope (228.1 mV dec^{-1} and 112.9 mV dec^{-1}) was observed with Co_3O_4/Ti and Co/Ti, respectively, consistent with their low HER activity. The remarkable HER catalytic performance of Co@NC/Ti (onset potential −56 mV, Tafel slope 78.2 mV dec^{-1}, current density 10 mA cm^{-2} at −106 mV) is very comparable to or even better than those of leading non-platinum HER catalysts in acidic aqueous electrolytes, such as MoS_2/reduced graphene (−100 mV, 41 mV dec^{-1}),[40] nickel–molybdenum nitride nanosheets (−78 mV, 35.9 mV dec^{-1}),[20] cobalt-embedded nitrogen-rich carbon nanotubes (−50 mV, 80 mV dec^{-1}),[41] and CoS_2 nanowire arrays (10 mA cm^{-2} at −145 mV).[24]

Interestingly, the Co@NC/Ti nanocomposites also exhibit an excellent HER activity in a wide range of pH including, for instance, strongly alkaline 1 M KOH (Fig. S5†) and neutral 0.1 M phosphate buffer (pH = 7, Fig. S6†).

Electrochemical impedance measurements were also carried out to characterize the interfacial electron-transfer kinetics involved in the HER. Fig. 4c shows the representative Nyquist plots of the Co@NC/Ti electrode at various overpotentials, where one can see that with increasing overpotential, the diameter of the arc shrank, implying a diminishment of the charge transfer resistance (R_{ct}). More detailed analyses were carried out by fitting the impedance data to an equivalent circuit (Fig. 4c, inset), where a constant phase element (CPE) was employed. The charge transfer resistance R_{ct} is related to the electrocatalysis kinetics and a lower value corresponds to a faster reaction rate. The values of R_{ct} were found to decrease significantly with increasingly negative potentials, from 26.7 Ω at −20 mV to 9.9 Ω at −100 mV.

The durability of Co@NC/Ti for the HER in 0.5 M H_2SO_4 was also examined. Fig. 4d shows the time dependent current

density curve for Co@NC/Ti at −150 mV. After 8 h of continuous operation, the current remained largely unchanged. As shown in the inset in Fig. 4d, after 1000 cycles of potential scans in 0.5 M H_2SO_4 at a scan rate of 100 mV s^{-1}, the polarization curve shows a negligible difference as compared to the initial one. In sharp contrast, both Co_3O_4/Ti and Co/Ti exhibited a poor stability in 0.5 M H_2SO_4 (Fig. S7†), where the corresponding current density diminished by 23.4% after 5 h of continuous operation and 74.1% after 3 h of continuous operation, respectively.

The superior HER catalytic performance and stability of the Co@NC/Ti electrode might be attributed to the following factors. (1) The direct growth of Co nanorods on the Ti mesh allowed the hybrids to possess high electrical conductivity, as confirmed by electrochemical impedance measurements (Fig. 4c) in which the uncompensated resistance R_s was only 1.3 Ω, thus eliminating the use of polymer binders and conductive additives; (2) the nanorod arrays entailed a large surface area and abundant exposed active sites. In fact, when the Co@NC arrays were scratched from the Ti mesh and deposited onto a glassy carbon disk electrode, good HER activity could still be seen (Fig. S8†), but the performance was much lower (*e.g.*, 10 mA cm^{-2} at −239 mV) than that of Co@NC/Ti (10 mA cm^{-2} at −106 mV); (3) Co likely played a crucial role in the HER, where it not only decreased the local work function on the carbon surface, but also changed the electronic density of states around the carbon such that the carbon atoms served as catalytic active sites.[28,29] (4) The overcoating shell of graphitized and amorphous carbon impeded electrochemical dissolution of cobalt in acid electrolytes, leading to improved stability of the Co@NC/Ti hybrid catalysts. In contrast, the unprotected Co_3O_4/Ti and Co/Ti hybrids exhibited only poor stability for the HER in 0.5 M H_2SO_4 (Fig. S7†).

In summary, N-doped carbon-coated Co nanorod arrays supported on a Ti mesh (Co@NC/Ti) were prepared by a two-step procedure that entailed hydrothermal growth of Co_3O_4 nanorod arrays on a Ti mesh, followed by reduction of Co_3O_4 to Co with a carbon overcoating layer by thermal decomposition of dicyanodiamine. Electrochemical studies showed that the obtained electrocatalysts exhibited an excellent HER activity with an onset potential of −56 mV (*vs.* RHE), a large current density (10 mA cm^{-2} at −106 mV), a small Tafel slope of 78.2 mV dec^{-1} and prominent electrochemical durability. The results presented herein may offer a new methodology for the design and engineering of effective HER catalysts based on earth-abundant and inexpensive components.

Acknowledgements

This work was supported by the National Recruitment Program of Global Experts, the PhD Start-up Funds of the Natural Science Foundation of Guangdong Province (S2013040016465), the Zhujiang New Stars of Science & Technology (2014J2200061) and the Fundamental Research Funds for Central Universities (x2hjD2131690).

Notes and references

1 E. Anxolabéhère-Mallart, C. Costentin, M. Fournier, S. Nowak, M. Robert and J.-M. Savéant, *J. Am. Chem. Soc.*, 2012, **134**, 6104–6107.
2 C. C. L. McCrory, C. Uyeda and J. C. Peters, *J. Am. Chem. Soc.*, 2012, **134**, 3164–3170.
3 R. Subbaraman, D. Tripkovic, D. Strmcnik, K.-C. Chang, M. Uchimura, A. P. Paulikas, V. Stamenkovic and N. M. Markovic, *Science*, 2011, **334**, 1256–1260.
4 C. He, X. Wu, J. Shen and P. K. Chu, *Nano Lett.*, 2012, **12**, 1545–1548.
5 M. L. Helm, M. P. Stewart, R. M. Bullock, M. R. DuBois and D. L. DuBois, *Science*, 2011, **333**, 863–866.
6 D. Kong, H. Wang, J. J. Cha, M. Pasta, K. J. Koski, J. Yao and Y. Cui, *Nano Lett.*, 2013, **13**, 1341–1347.
7 D. V. Esposito, S. T. Hunt, A. L. Stottlemyer, K. D. Dobson, B. E. McCandless, R. W. Birkmire and J. G. Chen, *Angew. Chem., Int. Ed.*, 2010, **122**, 10055–10058.
8 W.-F. Chen, K. Sasaki, C. Ma, A. I. Frenkel, N. Marinkovic, J. T. Muckerman, Y. Zhu and R. R. Adzic, *Angew. Chem., Int. Ed.*, 2012, **51**, 6131–6135.
9 A. B. Laursen, S. Kegnaes, S. Dahl and I. Chorkendorff, *Energy Environ. Sci.*, 2012, **5**, 5577–5591.
10 P. D. Tran, A. Le Goff, J. Heidkamp, B. Jousselme, N. Guillet, S. Palacin, H. Dau, M. Fontecave and V. Artero, *Angew. Chem., Int. Ed.*, 2011, **123**, 1407–1410.
11 R. K. Das, Y. Wang, S. V. Vasilyeva, E. Donoghue, I. Pucher, G. Kamenov, H.-P. Cheng and A. G. Rinzler, *ACS Nano*, 2014, **8**, 8447–8456.
12 W. Cui, Q. Liu, N. Cheng, A. M. Asiri and X. Sun, *Chem. Commun.*, 2014, **50**, 9340–9342.
13 Y. Zhao, F. Zhao, X. Wang, C. Xu, Z. Zhang, G. Shi and L. Qu, *Angew. Chem., Int. Ed.*, 2014, **53**, 13934–13939.
14 W. Zhou, K. Zhou, D. Hou, X. Liu, G. Li, Y. Sang, H. Liu, L. Li and S. Chen, *ACS Appl. Mater. Interfaces*, 2014, **6**, 14911–14918.
15 D. Gopalakrishnan, D. Damien and M. M. Shaijumon, *ACS Nano*, 2014, **8**, 5297–5303.
16 C.-B. Ma, X. Qi, B. Chen, S. Bao, Z. Yin, X.-J. Wu, Z. Luo, J. Wei, H.-L. Zhang and H. Zhang, *Nanoscale*, 2014, **6**, 5624–5629.
17 K. Zhou, W. Zhou, X. Liu, Y. Wang, J. Wan and S. Chen, *ACS Appl. Mater. Interfaces*, 2014, **6**, 14911–14918.
18 X. Ge, L. Chen, L. Zhang, Y. Wen, A. Hirata and M. Chen, *Adv. Mater.*, 2014, **26**, 3100–3104.
19 C. Wan, Y. N. Regmi and B. M. Leonard, *Angew. Chem., Int. Ed.*, 2014, **53**, 6407–6410.
20 W.-F. Chen, K. Sasaki, C. Ma, A. I. Frenkel, N. Marinkovic, J. T. Muckerman, Y. Zhu and R. R. Adzic, *Angew. Chem., Int. Ed.*, 2012, **51**, 6131–6135.
21 Z. Xing, Q. Liu, A. M. Asiri and X. Sun, *Adv. Mater.*, 2014, **26**, 5702–5707.
22 L. Cheng, W. Huang, Q. Gong, C. Liu, Z. Liu, Y. Li and H. Dai, *Angew. Chem., Int. Ed.*, 2014, **53**, 7860–7863.
23 D. Kong, H. Wang, Z. Lu and Y. Cui, *J. Am. Chem. Soc.*, 2014, **136**, 4897–4900.

24 M. S. Faber, R. Dziedzic, M. A. Lukowski, N. S. Kaiser, Q. Ding and S. Jin, *J. Am. Chem. Soc.*, 2014, **136**, 10053–10061.
25 J. Tian, Q. Liu, A. M. Asiri and X. Sun, *J. Am. Chem. Soc.*, 2014, **136**, 7587–7590.
26 E. J. Popczun, J. R. McKone, C. G. Read, A. J. Biacchi, A. M. Wiltrout, N. S. Lewis and R. E. Schaak, *J. Am. Chem. Soc.*, 2013, **135**, 9267–9270.
27 J. Tian, Q. Liu, N. Cheng, A. M. Asiri and X. Sun, *Angew. Chem., Int. Ed.*, 2014, **53**, 9577–9581.
28 X. Zou, X. Huang, A. Goswami, R. Silva, B. R. Sathe, E. Mikmeková and T. Asefa, *Angew. Chem., Int. Ed.*, 2014, **53**, 4372–4376.
29 J. Deng, P. Ren, D. Deng, L. Yu, F. Yang and X. Bao, *Energy Environ. Sci.*, 2014, **7**, 1919–1923.
30 J. Wang, D. Gao, G. Wang, S. Miao, H. Wu, J. Li and X. Bao, *J. Mater. Chem. A*, 2014, **2**, 20067–20074.
31 C. Zhou, Y. Zhang, Y. Li and J. Liu, *Nano Lett.*, 2013, **13**, 2078–2085.
32 P. Jiang, Q. Liu, Y. Liang, J. Tian, A. M. Asiri and X. Sun, *Angew. Chem., Int. Ed.*, 2014, **53**, 12855–12859.
33 W. Zhou, X. Cao, Z. Zeng, W. Shi, Y. Zhu, Q. Yan, H. Liu, J. Wang and H. Zhang, *Energy Environ. Sci.*, 2013, **6**, 2216–2221.
34 W. Zhou, X. Liu, Y. Sang, Z. Zhao, K. Zhou, H. Liu and S. Chen, *ACS Appl. Mater. Interfaces*, 2014, **6**, 4578–4586.
35 W. Zhou, X.-J. Wu, X. Cao, X. Huang, C. Tan, J. Tian, H. Liu, J. Wang and H. Zhang, *Energy Environ. Sci.*, 2013, **6**, 2921–2924.
36 D. Deng, L. Yu, X. Chen, G. Wang, L. Jin, X. Pan, J. Deng, G. Sun and X. Bao, *Angew. Chem., Int. Ed.*, 2013, **52**, 371–375.
37 Z. Wen, S. Ci, Y. Hou and J. Chen, *Angew. Chem., Int. Ed.*, 2014, **53**, 6496–6500.
38 L. Qu, Y. Liu, J.-B. Baek and L. Dai, *ACS Nano*, 2010, **4**, 1321–1326.
39 J. G. N. Thomas, *Trans. Faraday Soc.*, 1961, **57**, 1603–1611.
40 Y. Li, H. Wang, L. Xie, Y. Liang, G. Hong and H. Dai, *J. Am. Chem. Soc.*, 2011, **133**, 7296–7299.
41 X. Zou, X. Huang, A. Goswami, R. Silva, B. R. Sathe, E. Mikmeková and T. Asefa, *Angew. Chem., Int. Ed.*, 2014, **53**, 4372–4376.